SHIP TOWED BY KITE IN WAVES: A STRONGLY COUPLED SYSTEM

N. Bigi, ENSTA Bretagne, France, nedeleg.bigi@ensta-bretagne.org
J. B. Leroux, ENSTA Bretagne, France, jean-baptiste.leroux@ensta-bretagne.fr
K. Roncin, ENSTA Bretagne, France, kostia.roncin@ensta-bretagne.fr
A. Nême, ENSTA Bretagne, France, alain.neme@ensta-bretagne.fr
C. Jochum, ENSTA Bretagne, France, christian.jochum@ensta-bretagne.fr
Y. Parlier, beyond the sea, France, yves.parlier@beyond-the-sea.com

The auxiliary propulsion of ship towed by kite appears as an efficient concept to reduce CO_2 emmissions and fuel consumptions. Nevertheless, the influence of a kite may endanger a ship since a kite performs periodic dynamic flights. In order to anticipate and to evaluate the risks may due to a kite, simulations of a ship towed by kite are performed. Two approaches are developed: a frequency domain approach with a weak coupling between the kite and the ship, and a time domain approach with a strong coupling are developed. Both approaches are based on the Salvesen, Tuck and Faltinsen (STF) strip theory. Using the DTMB 5512 surface vessel combattant, it is shown that both approaches are consistent to the experimental fluid dynamic data and to the STF strip theory results. In calm water, the comparison between the time domain and the frequency domain approaches shows that with a kite excitation frequency near the natural roll frequency of the ship, a strong coupling in time domain is necessary regarding the roll motion. With a beam wave, the kite frequency excitation is highly modified. Consequently, a peak of excitation appears at the wave frequency which has an important influence on the roll amplitude.

NOMENCLATURE

$\mathbf{c}$	Current reference frame (inertial) $\left(O_c, \underline{x}_c, \underline{y}_c, \underline{z}_c\right)$	(–)
$\mathbf{n}$	Earth fixed reference frame (inertial) $\left(O_n, \underline{x}_n, \underline{y}_n, \underline{z}_n\right)$	(–)
$\mathbf{rw}$	Relative wind frame $\left(\underline{x}_{rw}, \underline{y}_{rw}, \underline{z}_{rw}\right)$	(–)
$\mathbf{s}$	Ship fixed frame $\left(O_s, \underline{x}_s, \underline{y}_s, \underline{z}_s\right)$	(–)
ω	Frequency of the motion	(rad.s^{-1})
ψ_w	Wave direction with respect to the $\mathbf{c}frame$	(rad)
$\underline{\xi}$	Generalized velocity vector of a point H fixed to the ship with respect to the $\mathbf{h}$ frame expressed in the $\mathbf{h}$ frame	(m.s^{-1}, rad.s^{-1})
$\underline{S}$	Generalized position vector of the ship iwth respect to the $\mathbf{c}$ frame expressed in the $\mathbf{c}$ frame	(m, rad)
$\underline{U}_a$	Kite attachment point velocity	(m.s^{-1})
$\underline{U}_h$	Mean ship forward speed	(m.s^{-1})
$\underline{U}_k$	Kite velocity with respect to the $\mathbf{rw}$ frame	(m.s^{-1})
$\underline{U}_{aw}$	Apparent wind velocity to the kite	(m.s^{-1})
$\underline{U}_c$	Current velocity with respect to the $\mathbf{n}$ frame	(m.s^{-1})
$\underline{U}_{rw}$	Relative wind velocity	(m.s^{-1})
$\underline{U}_{tw}$	True wind velocity	(m.s^{-1})
$\underline{V}_s$	Generalized velocity vector of the ship at O_s with respect to the $\mathbf{c}$ frame expressed in the $\mathbf{s}$ frame	(m.s^{-1}, rad.s^{-1})
g	Gravitational constant (9.81)	(m.s^{-2})
K	Kite position	(m)
k	Wave number	(m^{-1})
L_t	Tether length	(m)
l_z	Vertical position of O_s with respect to the baseline	(m)
n	Wind gradient parameter	(–)
S	Wave spectrum	(–)
z_{ref}	Measurement altitude of the wind	(m)
dof	Degree(s) of freedom	(–)
EFD	Experimental Fluid Dynamic	

1 INTRODUCTION

This work is part of the beyond the sea® research program leaned by the IRDL laboratory at ENSTA Bretagne. The project attempts to develop tethered kite system as an auxiliary device to the propulsion of merchant ships. The existing knowledge on ships towed by kite has demonstrated great prospects for this technology in term of CO_2 emissions and fuel savings. However, studies on the limitations of this concept to guarantee the safety and the integrity of the ship are very limited.

According to the literature, Leloup et al. [1] and Naaijen et al. [2], these fuel consumption studies have been carried out with an arbitrary kite surface. Indeed, no kite design criteria according to ship characteristics were studied formerly.

These kite design limits should be explored through the interactions between the ship and the kite. The motions of such a system are highly dynamic since a kite experiences a periodic dynamic flight. In Bigi et al. [3], the influence of the kite attachment point on the deck has been investigated on a fishing vessel equipped with a kite. This study was limited to the horizontal ship motions, surge, sway and yaw, by means of a maneuvering model in calm water. Nevertheless, even if the water was supposed to be calm, the work in [3] suffers a priori of two critical assumptions: the effect of the vertical ship motions on the horizontal ship motions have been neglected, and the influence of the frequency of the kite excitations on the ship motions have been neglected. Since the hydrodynamic response of a structure depends strongly on the frequency of the excitation, the frequency of the kite excitation may have a strong influence on the ship motions.

A ship sailing in waves is commonly studied with seakeeping code based on the potential flow theory under the assumption of linear response of the ship to a given perturbation on a mean path. These studies are usually performed into the frequency domain in order to take benefit from the linear formulation to sum the motions. Nevertheless, since the kite and the ship may be strongly coupled, their interactions cannot be directly computed through a spectral description of the kite excitation. Consequently, the computation of the ship motions due to the kite into the frequency domain is limited to a weak coupling between the kite and the ship. In order to perform a strong coupling between the kite and the ship a time domain formulation is required. The aim of this paper is to assess the importance to take into account the coupling between the kite and the ship motions.

As highlighted by Skejic in [4], fast time-domain methods able to compute the 6 degrees of freedom (dof) combining horizontal and vertical motions of a ship are the linear convolution based methods. The linear convolution based method applied to the ship motions has been introduced by Cummins [5] in 1962 in order to take into account any type of excitation. Later, Bailey et al. [6] developed a method based on the linear convolution method and unifying the maneuvering motions and the seakeeping motions. Kristiansen and Egeland [7] and Fossen and Smogeli [8] introduced a state-space system method to compute the linear convolution integral of the Cummins equation of ship motion. Based on these developments, the linear convolution based method is fast to compute and close to the real-time on a classical computer. Therefore, the convolution based method is suitable for design purposes and is applied in this paper.

Regarding the kite modeling, different approaches are possible. A kite is ordinary composed of soft and light material such as fabric. The kite shape is basically dependent of its aerodynamic loading. An ideal kite model should take into account the complete fluid structure interaction. Nevertheless, a kite is very lightweight structure compared to its aerodynamic loading. Consequently, numerous studies on the dynamic kite flight motions have been carried out with the so-called zero-mass model (Wellicome and Wilkinson [9], Naaijen et al. [2], Dadd et al. [10] and Leloup et al. [1]). This model is fast to compute and is retained in this paper.

First the dynamic ship model, the kite model and the coupling between the ship and kite are introduced for the time domain and the time domain. Secondly, a validation of the ship model in head waves regarding heave and pitch motions is presented. These comparisons are based on the experimental fluid dynamic (EFD) of the surface vessel combatant DTMB 5512 provided by the University of Iowa [11] and studied by Irvine et al. [12]. Using the DTMB 5512 at full scale, the ship motions due to a kite on a crosswind path in calm water and with a beam wave are computed with the frequency domain approach and with the time domain approach. Finally, the results are compared and discussed.

2 MATHEMATICAL MODEL

2.1 REFERENCE FRAME AND PARAMETRISATION

The reference frames $\mathbf{n}$, $\mathbf{c}$, $\mathbf{s}$ and $\mathbf{h}$ are sketched in Fig. 1.

$\mathbf{n}$ is a earth fixed reference frame centered on O_n with $\underline{z}_n$ pointing downward. The current frame $\mathbf{c}$, centered on O_c, is translating at a constant speed $\underline{U}_c$ with respect to the $\mathbf{n}$ frame. The $\mathbf{c}$ frame is an inertial frame. $\underline{U}_c$ is orthogonal to $\underline{z}_n$. $\mathbf{s}$ is the ship fixed frame, $\underline{x}_s$ is pointing forward in the ship symmetry plane, $\underline{z}_s$ is pointing downward and $\underline{y}_s$ completes the direct orthogonal basis. $\underline{z}_s$ is normal to free surface when the ship is at the equilibrium. The origin of $\mathbf{s}$ denoted by O_s is in the ship symmetry plane at midship and at a vertical position from the baseline l_z.

The generalized position vector of the ship denoted by $\underline{S} = [s_x,\ s_y,\ s_z,\ \phi_s,\ \theta_s,\ \psi_s]^T$ is the assembly of the position of O_s and the ship Euler's angles with respect to the $\mathbf{c}$ frame. The generalized ship velocity at O_s expressed in $\mathbf{s}$ with respect to the $\mathbf{c}$ frame is denoted by $\underline{V}_s = [u_s,\ v_s,\ w_s,\ p_s,\ q_s,\ r_s]^T$, where the first three components are the linear velocities and the last three components are the turning rates. The transformation of a vector expressed in the $\mathbf{s}$ frame denoted by $\underline{n}^{(\mathbf{s})}$ can be expressed is the $\mathbf{c}$ frame with $\underline{n}^{(\mathbf{c})} = \underline{\underline{T}}^{\mathbf{c}}_{\mathbf{s}} \underline{n}^{(\mathbf{s})}$, where $\underline{\underline{T}}^{\mathbf{c}}_{\mathbf{s}}$ is the direct cosine matrix (cf. Eq. (1)).

$$\underline{\underline{T}}^{\mathbf{c}}_{\mathbf{s}} = \begin{bmatrix} \mathrm{c}\psi_s\mathrm{c}\theta_s & -\mathrm{s}\psi_s\mathrm{c}\phi_s + \mathrm{c}\psi_s\mathrm{s}\theta_s\mathrm{s}\phi_s & \mathrm{s}\psi_s\mathrm{s}\phi_s + \mathrm{c}\psi_s\mathrm{c}\phi_s\mathrm{s}\theta_s \\ \mathrm{s}\psi_s\mathrm{c}\theta_s & \mathrm{c}\psi_s\mathrm{c}\phi_s + \mathrm{s}\phi_s\mathrm{s}\theta_s\mathrm{s}\psi_s & -\mathrm{c}\psi_s\mathrm{s}\phi_s + \mathrm{s}\theta_s\mathrm{s}\psi_s\mathrm{c}\phi_s \\ -\mathrm{s}\theta_s & \mathrm{c}\theta_s\mathrm{s}\phi_s & \mathrm{c}\theta_s\mathrm{c}\phi_s \end{bmatrix}, \quad (1)$$

where, c and s denote the cosine and the sinus functions. The turning rates and the time derivatives of the ship Euler's angles satisfy the following relationship:

$$\begin{bmatrix} p_s \\ q_s \\ r_s \end{bmatrix} = \underline{\underline{R}}^{\mathbf{s}}_{\mathbf{c}} \begin{bmatrix} \dot{\phi}_s \\ \dot{\theta}_s \\ \dot{\psi}_s \end{bmatrix}, \quad (2)$$

where,

$$\underline{\underline{R}}^{\mathbf{s}}_{\mathbf{c}} = \begin{bmatrix} 1 & 0 & -\mathrm{s}\theta_s \\ 0 & \mathrm{c}\phi_s & \mathrm{c}\theta_s\mathrm{s}\phi_s \\ 0 & -\mathrm{s}\phi_s & \mathrm{c}\phi_s\mathrm{c}\theta_s \end{bmatrix}. \quad (3)$$

$\mathbf{h}$ is the hydrodynamic frame used by the seakeeping theory. The $\mathbf{h}$ frame centered on O_h can be considered as Galilean since $\mathbf{h}$ moves at the constant mean ship forward

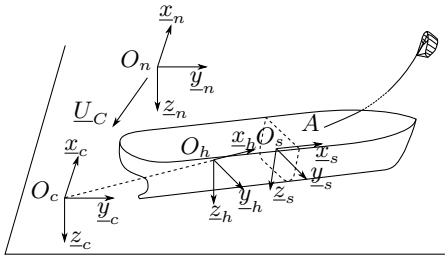

Figure 1: Earth fixed reference frame $\mathbf{n}$; hydrodynamic reference frame $\mathbf{h}$; ship fixed reference frame $\mathbf{s}$

speed U_h on a straight path compared to the current reference frame $\mathbf{c}$. At the ship equilibrium, we have $\left[\underline{x}_h,\, \underline{y}_h,\, \underline{z}_h\right] = \left[\underline{x}_s,\, \underline{y}_s,\, \underline{z}_s\right]$ and $O_h = H$, with $\underline{O_sH} = [d_x,\, 0,\, d_z]^T$ with respect to the $\mathbf{s}$ frame.

The generalized ship position vector of H expressed in the $\mathbf{h}$ frame is denoted by $\underline{\xi} = [\xi_1,\, \xi_2,\, \xi_3,\, \xi_4,\, \xi_5,\, \xi_6]^T$, where the first three components are the distance between O_h and the point H fixed to the ship. The three last components are the Euler's angle of the ship with respect to the $\mathbf{h}$ frame.

Fig. 2 illustrates the notations used for the zero-mass model. K denotes the kite position. $\mathbf{rw}$ is the relative wind coordinates system fixed to the tether attachment point A, moving at the velocity $\underline{U}_a$. The relative wind velocity $\underline{U}_{rw}$ defined in Eq. (4) is the difference between the true wind velocity $\underline{U}_{tw}$ at the kite location and the velocity of the tether attachment point compared to $\mathbf{n}$.

$$\underline{U}_{rw} = \underline{U}_{tw} - \underline{U}_a - \underline{U}_c \tag{4}$$

The direction of the relative wind velocity is $\underline{x}_{rw}$. $\underline{y}_{rw}$ is defined as: $\underline{y}_{rw} = \frac{\underline{z}_0 \times \underline{x}_{rw}}{\left\|\underline{z}_0 \times \underline{x}_{rw}\right\|}$. In order to define a direct orthonormal coordinates system, $\underline{z}_{rw}$ is defined as follows: $\underline{z}_{rw} = \underline{x}_{rw} \times \underline{y}_{rw}$.

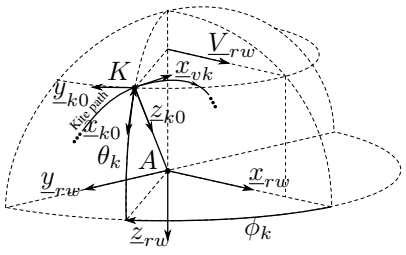

Figure 2: Coordinate systems used for the development of the zero-mass model

The apparent kite wind velocity is denoted by $\underline{U}_{aw}$ and can be expressed as follows:

$$\underline{U}_{aw} = \underline{U}_{rw} - \underline{U}_k, \tag{5}$$

where $\underline{U}_k$ denotes the kite velocity with respect to the $\mathbf{rw}$ frame.

2.2 SHIP MODELING

2.2.1 Time Domain Ship Equation of Motion

The starting point of the mathematical model is the frequency domain equation of motion, Eq. (6), use by the seakeeping theory:

$$\left[\underline{\underline{M}}_S^* + \underline{\underline{A}}^*\right] \ddot{\underline{\xi}} + \underline{\underline{B}}^* \dot{\underline{\xi}} + \underline{\underline{C}}^* \underline{\xi} = \underline{F}^* - \bar{\underline{F}}^*, \tag{6}$$

where, $\underline{\underline{M}}_S^*$, $\underline{\underline{A}}^*$, $\underline{\underline{B}}^*$ and $\underline{\underline{C}}^*$ denote respectively the generalized mass matrix, added mass matrix, damping matrix and restoring matrix with respect to the $\mathbf{h}$ frame. $\underline{F}^*$ denotes the sum of the generalized external forces (forces and moments) applied to the ship expressed in the $\mathbf{h}$ frame. $\bar{\underline{F}}^*$ is the mean value of $\underline{F}^*$.

It should be noticed that Eq. (6) holds only for a given frequency, ω, with small amplitude sinusoidal motions. Indeed, $\underline{\underline{A}}^*$and $\underline{\underline{B}}^*$ are frequency dependent. Consequently, this assumption leads to the following relationship:

$$\ddot{\underline{\xi}} = -\omega^2 \underline{\xi} \tag{7}$$

And, the direct cosine matrix between the $\mathbf{h}$ frame and the $\mathbf{s}$ frame can be simplified considering small angles of oscillations:

$$\underline{\underline{T}}_{\mathbf{s}}^{\mathbf{h}} = \begin{bmatrix} 1 & -\xi_6 & \xi_5 \\ \xi_6 & 1 & -\xi_4 \\ -\xi_5 & \xi_4 & 1 \end{bmatrix} \tag{8}$$

Defining $\delta\underline{V}_s = [u_s - U_h,\, v_s,\, w_s,\, p_s,\, q_s,\, r_s]^T$, $\underline{\xi}$ can be expressed in term of $\delta\underline{V}_s$ with Eq. (9). The detailed of this transformation was presented in [13].

$$\begin{cases} \dot{\underline{\xi}} = & \underline{\underline{J}}\delta\underline{V}_s - \frac{U}{\omega_e^2}\underline{\underline{L}}\delta\dot{\underline{V}}_s \\ \ddot{\underline{\xi}} = & \underline{\underline{J}}\delta\dot{\underline{V}}_s + U\underline{\underline{L}}\delta\underline{V}_s \end{cases}, \tag{9}$$

where,

$$\underline{\underline{J}} = \begin{bmatrix} 1 & 0 & 0 & 0 & z_H & 0 \\ 0 & 1 & 0 & -z_H & 0 & x_H \\ 0 & 0 & 1 & 0 & -x_H & 0 \\ 0 & 0 & 0 & 1 & 0 & 0 \\ 0 & 0 & 0 & 0 & 1 & 0 \\ 0 & 0 & 0 & 0 & 0 & 1 \end{bmatrix}, \tag{10}$$

and,

$$\underline{\underline{L}} = \begin{bmatrix} 0 & 0 & 0 & 0 & 0 & 0 \\ 0 & 0 & 0 & 0 & 0 & 1 \\ 0 & 0 & 0 & 0 & -1 & 0 \\ 0 & 0 & 0 & 0 & 0 & 0 \\ 0 & 0 & 0 & 0 & 0 & 0 \\ 0 & 0 & 0 & 0 & 0 & 0 \end{bmatrix}. \tag{11}$$

Then, using Eq. (9) the equation of motion Eq. (6) can be expressed in term of $\delta\underline{V}$ as follows:

$$\left[\underline{\underline{M}}_S + \underline{\underline{A}}\right] \delta\dot{\underline{V}}_s + \left[\underline{\underline{B}} + \underline{\underline{D}}\right] \delta\underline{V}_s + \underline{\underline{C}}\, \underline{\xi} = \underline{F} - \bar{\underline{F}}, \tag{12}$$

where,

$$\begin{cases} \underline{\underline{M}}_S & = \underline{\underline{J}}^T \underline{\underline{M}}^*_S \underline{\underline{J}} \\ \underline{\underline{A}} & = \underline{\underline{J}}^T \underline{\underline{A}}^* \underline{\underline{J}} \\ \underline{\underline{D}} & = \underline{\underline{J}}^T \underline{\underline{M}}^*_S \underline{\underline{L}} \\ \underline{\underline{B}} & = \underline{\underline{J}}^T \left[\underline{\underline{B}}^* + U_h \underline{\underline{A}}^* \underline{\underline{L}} \right] \underline{\underline{J}} \\ \underline{\underline{C}} & = \underline{\underline{J}}^T \underline{\underline{C}}^* \\ \underline{\underline{F}} & = \underline{\underline{J}}^T \underline{\underline{F}}^* \end{cases} \tag{13}$$

Equation (12) can be solved directly into the frequency domain.

Nevertheless, since a kite and a ship may have strong coupled motions, it may be preferable to transform Eq. (12) into the time domain using the impulse response function as Cummins [5], Ogilvie [14] and Fossen [8]. Moreover, it is not convenient to use the parametrisation in $\delta \underline{V}$. The steady state corresponds to $u_s = U_h$ and $\delta \underline{V}_s = \underline{0}$. Due to the special structure of $\underline{\underline{C}}$, it can be noticed that $\underline{\underline{C}}\ \underline{\xi} = \underline{\underline{C}}\ \underline{S}$. Consequently, the ship equation of motion for arbitrary motions and using the parametrisation in $\underline{V}_s$ is:

$$\left[\underline{\underline{M}}_S + \underline{\underline{\tilde{A}}} \right] \underline{\dot{V}}_s + \left[\underline{\underline{\tilde{B}}} + \underline{\underline{D}} \right] \underline{V}_s + \underline{\mu} + \underline{\underline{C}}\ \underline{S} = \underline{F}, \tag{14}$$

where, $\underline{\underline{\tilde{A}}} = \lim_{\omega \to +\infty} \underline{\underline{A}}(\omega)$ and $\underline{\underline{\tilde{B}}} = \lim_{\omega \to +\infty} \underline{\underline{B}}(\omega)$. $\underline{\mu}$ is defined as follows:

$$\underline{\mu} = \int_0^t \underline{\underline{K}}(t-\tau)\, \delta \underline{V}_s(\tau)\, d\tau, \tag{15}$$

where $\underline{\underline{K}}$ denotes the retardation matrix. Strictly speaking, the left boundary of the convolution term should be $-\infty$. However, for causal system the left boundary can be replaced by 0. The retardation matrix can be identified with Eq. (6) assuming sinusoidal motions in Eq. (14).

$$\underline{\underline{K}}(j\omega) = \underline{\underline{B}}(\omega) - \underline{\underline{\tilde{B}}} + j\omega \left[\underline{\underline{A}}(\omega) - \underline{\underline{\tilde{A}}} \right], \tag{16}$$

where $j^2 = -1$.

The infinite added mass and damping matrix are estimated according to the STF strip theory [15] where $\underline{\underline{A}}$ and $\underline{\underline{B}}$ are expressed in terms of sections added mass and damping. The 2D sections damping at infinite frequency is zero. This theoritical result is proven in [16] assuming a potential flow. The 2D sections infinite added mass are evaluated with the higher frequency computed, which is justified since the added mass remain almost constant at high frequency.

2.2.2 Computation of the Hydrodynamic Data and of the Convolution Term with a State Space System

The computation of convolution product is very time consuming. However, each convolution component $\mu_{i \in [\![1,6]\!]}$ can be approximated by a state space system in Eq. (17), as introduced by Kristiansen and Egeland in [7].

$$\begin{array}{c} \mu_i \\ \approx \\ \begin{cases} \mu_i & = \sum_{j=1}^{6} \mu_{ij} \\ \underline{\dot{y}}_{ij} & = \underline{\underline{A}}'_{ij} \underline{y}_{ij} + \underline{B}'_{ij} V_{s,j} \\ \mu_{ij} & = \underline{\underline{C}}'_{ij} \underline{y}_{ij} \end{cases} \end{array}, \tag{17}$$

where, $\left\{ \underline{\underline{A}}'_{ij},\ \underline{B}'_{ij},\ \underline{\underline{C}}'_{ij} \right\}$ represents the state-space model corresponding to a transfer function denoted by H_{ij} fitting $K_{ij}(j\omega)$, for $i, j \in [\![1,6]\!]$. $K_{ij}(j\omega)$ are obtained with the added mass and damping. The frequency range depends on the ship size, but the low frequency limit is generally 0.1 rad.s^{-1} and the high frequency limit does not generally exceed 10 rad.s^{-1}. The identification of H_{ij} can be identified either into the frequency domain or into the time domain, see [17].

In this paper, the identification procedure is done in two steps. The first step consists in identifying the transfert function H_{ij} into the time domain via the singular value decomposition method proposed by Kung [18]. This step is performed with the help of the Matlab® function "imp2ss". This operation is repeated for several orders, for instance from 2 to 10. The best order is selected taking into account the spectrum and the impulse response of H_{ij} compared to K_{ij}. The second step consists in setting the form of the transfert function according to the K_{ij} properties described in [17]. K_{ij} should tends towards zero at low and infinite frequencies. According to the initial time value of the impulse response, the difference between the order of the denominator and the numerator must be 1. According to the zero final time value of the impulse response function K_{ij}, the term with an order equal to zero at the numerator must be zero. Consequently, the transfert function H_{ij} has the following form:

$$H_{ij} = \frac{K_{ij}(t=0)\, p^{n-1} + \ldots + a_1 p}{p^n + b_{n-1} p^{n-1} + \ldots + b_0} \tag{18}$$

Setting this form to the best order selected at the first step, the free coefficients are optimized with the frequency data.

It should be noticed that the first step of the identification procedure results are improved in term of spectrum when the data are extrapolated at high frequency. Therefore the damping B^*_{ij} is extrapolated with the function in Eq. 19, proposed by Greenhow [19]:

$$B^*_{ij}(\omega) - B^*_{ij}(\infty) = \frac{\beta_1}{\omega^4} + \frac{\beta_2}{\omega^2}, \tag{19}$$

where β_1 and β_2 are two constants chosen in order to provide continuity and derivability.

2.2.3 Wave Forces

The Froude-Krilov and diffraction forces are obtained with the STF 2D strip theory [15], with the Shipmo software. Assuming an infinite depth, the dispersion relationship is $kg = \omega^2$, where k denotes the wave number. Thus the frequency of

encounter denoted by ω_e can be approximated by the following relationship:

$$\omega_e = \omega - \frac{u_s}{g}\omega^2 \cos\beta_w \tag{20}$$

where ω and β_w denote respectively the wave frequency (in rad.s^{-1}) and the angle of the waves with respect to the ship heading. β_w can be approximated by $\beta_w = \psi_s - \psi_w$, where ψ_w denotes the wave angle with respect to $\underline{x}_c$. The expression of the Froude-Krilov and diffraction forces generated by a single unitary wave can be expressed by the following expression:

$$\begin{aligned}\underline{f}_w\left(u_s,\psi_s,\omega,\psi_w\right) = \left\|\underline{f}_w\left(u_s,\omega,\beta_w\right)\right\| \\ \cos\left[k\cos\left(\psi_w\right)s_x + k\sin\left(\psi_w\right)s_y - \omega t \right. \\ \left. -\phi\left(u_s,\omega,\beta_w\right)+\epsilon\right]\end{aligned} \tag{21}$$

For any wave wave spectrum $S\left(\omega,\psi_w\right)$, the Froude-Krilov and diffraction forces can be expressed as follows:

$$\begin{aligned}&\underline{F}_w\left(u_s,\psi_s\right) = \\ &\sum_{i=1}^{N}\sqrt{2S\left(\omega_i,\psi_{w,i}\right)\Delta\psi_w\Delta\omega}\,\underline{f}_w\left(u_s,\psi_s,\omega_i,\psi_{w,i},\epsilon_i\right)\end{aligned} \tag{22}$$

where ϵ_i is a random phase equidistributed between 0 and 2π in order to obtain a Gaussian wave spectrum.

2.3 KITE MODELING

According to the zero-mass model, the masses of the tether and the kite are neglected and the tether is assumed to be straight and of constant length L_t. Consequently, the kite velocity with respect to the $\mathbf{rw}$ frame is normal to $\underline{z}_{k0}$ and for any configurations the tether tension is opposed to the aerodynamic kite force:

$$\underline{f}^{(t)} = \underline{f}_{aero/K} \tag{23}$$

Assuming that the kite flight with a constant lift to drag ratio and that the apparent wind velocity is in its symmetry plane, Leloup et al. [1] expressed the kite velocity according to a given kite velocity direction $\underline{x}_{vk}$ in Eq. (24):

$$\begin{aligned}\underline{U}_k = U_{rw}\left(\underline{x}_{vk}\cdot\underline{x}_{rw}\right)\underline{x}_{vk} + \\ U_{rw}\sqrt{\left(\underline{x}_{vk}\cdot\underline{x}_{rw}\right)^2 + \left(\frac{\underline{z}_{k0}\cdot\underline{x}_{rw}}{\sin\epsilon_k}\right)^2 - 1}\underline{x}_{vk}\end{aligned} \tag{24}$$

Then, the tether tension is given by the following formula:

$$\underline{T}_k = -\frac{C_{L_K}\rho_a A_k U_{aw}^2}{2\cos\epsilon_k}\underline{z}_{k0} \tag{25}$$

The generalized tether force vector acting on the ship at O_S with respect to $\mathbf{s}$ frame is expressed as follows:

$$\underline{F}_k = \left[\begin{array}{cc}\underline{T}_k^{(\mathbf{s})} & \underline{O_S A}^{(\mathbf{s})}\times\underline{T}_K^{(\mathbf{s})}\end{array}\right]^T \tag{26}$$

In order to represent the wind friction with the sea, the true wind velocity $\underline{U}_{tw}$ is function of the altitude according to the wind gradient law recommended by the ITTC [20]. The measurement altitude of the wind relative to the sea level is denoted by z_{ref}. The wind velocity at z_{ref} is denoted by $\underline{U}_{ref}$. The wind gradient parameter n is equal to $1/7$ as recommended by [20].

$$\underline{U}_{tw} = \left(\underline{U}_{ref} - \underline{U}_c\right)\left(\frac{z_k^{(\mathbf{n})}}{z_{ref}^{(\mathbf{n})}}\right)^n + \underline{U}_c \tag{27}$$

2.4 KITE CONTROL

The kite velocity direction $\underline{x}_{VK}$ is controlled in order to follow a trajectory denoted by $\mathcal{C}_k$. At each time step of the simulation, the kite velocity direction is defined by the target point $\tilde{K}$ expressed as follows:

$$\tilde{K} = \mathcal{C}_k\left(\lambda + \|\underline{U}_k\|\,dt\right), \tag{28}$$

where λ is the curvilinear abscissa of the closest point of $\mathcal{C}_k$ from the current kite position. θ_{ref} and ϕ_{ref} are the elevation and azimuth of the trajectory on the sphere of center A and radius L_t. In order to perform "eight" trajectories, θ_{ref} and ϕ_{ref} are defined as follows:

$$\begin{cases}\theta_{ref} & = \Delta\theta_8\sin\left(2\lambda\right) + \theta_8 \\ \phi_{ref} & = \Delta\phi_8\sin(\lambda) + \phi_8\end{cases}, \tag{29}$$

where, $\lambda \in [0; 2\pi]$ and $\left(\ \phi_8,\ \theta_8\ \right)$ is the elevation and the azimuth of the center of the trajectory denoted by C_8. This trajectory is defined into the $\mathbf{rw}$ frame. At elevation θ_k and azimuth ϕ_k on a sphere of radius L_t, the corresponding Cartesian coordinates of the kite in $\mathbf{rw}$ frame are defined as follows:

$$\underline{K}^{(\mathbf{rw})} = \left[\begin{array}{c}L_T\cos\theta_K\cos\phi_K \\ L_T\cos\theta_K\sin\phi_K \\ -L_T\sin\theta_K\end{array}\right] \tag{30}$$

The eight trajectories can be rotated by an angle χ_8 around $\underline{C_8 A}$.

2.5 TIME AND FREQUENCY COMPUTATION

2.5.1 Time Domain

The equations describing the motion of the system can be transformed into a system of first order differential equations Eq. (31). This system is obtained with Eqns. (1, 2, 14, 17, 24).

$$\begin{cases}\dot{\underline{S}} & = \begin{bmatrix}\underline{\underline{T}}_{\mathbf{s}}^{\mathbf{c}} & \underline{\underline{0}} \\ \underline{\underline{0}} & \underline{\underline{R}}_{\mathbf{s}}^{\mathbf{c}}\end{bmatrix}\underline{V} \\ \dot{\underline{V}} & = \left[\underline{\underline{M}}_S + \underline{\underline{\tilde{A}}}\right]^{-1}\left[\underline{F} - \left[\underline{\underline{\tilde{B}}} + \underline{\underline{D}}\right]\underline{V} - \underline{\mu} - \underline{\underline{C}}\,\underline{S}\right] \\ \dot{\underline{y}}_{ij} & = \underline{\underline{A}}_{ij}^{'}\underline{y}_{ij} + \underline{\underline{B}}_{ij}^{'}V_j,\ \forall i,j\in[\![1;6]\!] \\ \dot{\underline{K}}^{(\mathbf{c})} & = U_{rw}\left(\underline{x}_{vk}\cdot\underline{x}_{rw}\right)\underline{x}_{vk}^{(\mathbf{c})} + \underline{U}_A^{(\mathbf{c})} \\ & \quad + U_{rw}\sqrt{\left(\underline{x}_{vk}\cdot\underline{x}_{rw}\right)^2 + \left(\frac{\underline{z}_{k0}\cdot\underline{x}_{rw}}{\sin\epsilon_k}\right)^2 - 1}\,\underline{x}_{vk}^{(\mathbf{c})}\end{cases} \tag{31}$$

Equation (31) represents 12 scalar equations for the ship and 3 scalar equations for the kite and 75 scalars equations

for the convolution term assuming that the order of each state space model is 5 and taking into account the ship symmetry. Thus, with the presented model, a ship towed by kite is described by approximately 100 scalar equations depending on the orders of the state space model. With the time domain approach, the full coupling between the ship motions and the kite motions is solved. Thus, the coupling between the kite and the ship can be qualified of strong.

This system of differential equations is numerically integrated with a Runge-Kutta scheme of order 4 with fixed time step.

2.5.2 Frequency Domain

The ship motions into the frequency domain can be computed according to Eq. (6) or Eq. (12). The two formulation are perfectly equivalent. Here, in order to perform a consistent comparison with the time domain formulation, Eq. (12) is prefered since the frequency dependent added mass and damping matrix can be obtained with the fitted retardation matrix Eq. (16). Indeed, with Eq. (12), the frequency dependent added mass and damping matrix are given by the following expression:

$$\begin{cases} A_{ij} = & \frac{1}{\omega}\Im\left(H_{ij}\right) + \tilde{A}_{ij} \\ B_{ij} = & \Re\left(H_{ij}\right) + \tilde{B}_{ij} \end{cases}, \tag{32}$$

where, $\Re$ and $\Im$ denote respectively the real part and the imaginary part. Assuming harmonic excitations, $\underline{F} - \bar{\underline{F}} = \Re\left[\underline{f}\exp\left(-j\omega t - j\phi\right)\right]$, $\underline{S}$ is of the form $\underline{S} = \Re\left[\underline{s}\exp\left(-j\omega t\right)\right]$. Then Eq. (12) is solved for each frequency.

The kite excitation spectrum is computed by means of fast fourier transform (FFT) of the kite forces computed with a mean ship speed. Consequently, no interaction between the kite and the motions is taken into account. With the frequency domain approach, the coupling between the ship and the kite can be considered weak.

3 SHIP MODEL VALIDATION CASE

The presented ship model is validated with experimental fluid dynamic (EFD) data and with STF strip theory results on the David Taylor Model Basin (DTMB) 5512. The experimental data are provided by the University of Iowa [11] and are presented in Irvine et al. [12]. The EFD data concerns the heave and pitch motions in regular head waves, with and without forward speed. The STF strip theory is computed with the Shipmo software distributed by the Marin®.

The DTMB model 5512 is a 1:46.6 scale model. The hull form and its characteristics are respectively plotted in Fig. 3 and summarized in Tab 1.

The computed ship motions are performed at zero forward speed and at a Froud number of 0.28 which corresponds to $U = 1.53$ m.s^{-1} and with frequency head waves, ω_0, from 1 rad.s^{-1} to 7.5 rad.s^{-1}. Figures 4 and 5 plot the Response Amplitude Operator (RAO) for the pitch and the heave motions obtained with the experimental data, with the STF strip theory and with the presented model. The experimental data are obtained for different wave steepness $s_w = \{0.025,\ 0.05,\ 0.075\}$. The RAO amplitude for heave motion is directly the ratio of the heave amplitude motion to the wave amplitude. The RAO amplitude for the pitch motion is given by the ratio of the pitch motion amplitude (in radian) to the wave amplitude multiplied by the wave number k. The phase angle of the presented model is obtained by cross correlation between the free surface elevation and the ship motion time series.

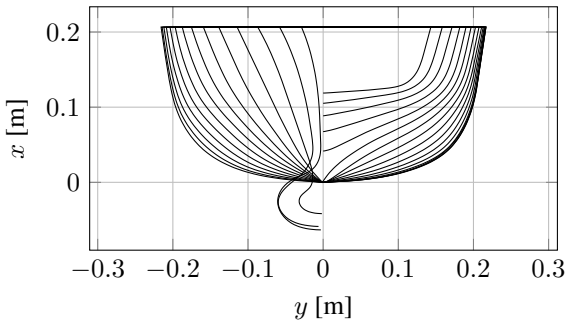

Figure 3: DTMB 5512 hull sections

Parameter	Units	5512	Full Scale
Scale ratio	-	46.6	1
Length, L_{pp}	m	3.048	142.04
Beam, B	m	0.405	18.87
Draft, T	m	0.132	6.15
Weight	Kg - t	86.6	8763.5
LCG	m	1.536	71.58
VCG	m	0.162	7.55
Pitch radius of gyration, k_5	m	0.764	35.6

Table 1: DTMB 5512 hull and full scale characteristics

Concerning the amplitude, an overall good agreement is found with and without forward speed between the EFD data, the STF strip theory, the time domain and the frequency domain models. The influence of the wave steepness on the EFD data is not significant. This shows that the wave conditions comply with the first order potential flow formulation of the STF strip theory.

As it is theoritically expected, the frequency domain and the time domain approach match perfectly for the amplitude. Very small differences can be observed in term of phase angle, but these differences are probably caused to the postraitement method. This shows that the frequency domain approach and the time domain approach are equivalent for a single frequency excitation. The two approaches are very close to the STF strip theory. The differences with the STF strip theory are due to the approximations performed with the identification method of the transfer functions H_{ij}.

As a conclusion, the very small differences between the STF strip theory and the presented models in Figs. 4 and 5 show that the transformation of the equation of motion into the s frame and the identification methods for the infinite added mass and damping matrix and the state-space model are consistent.

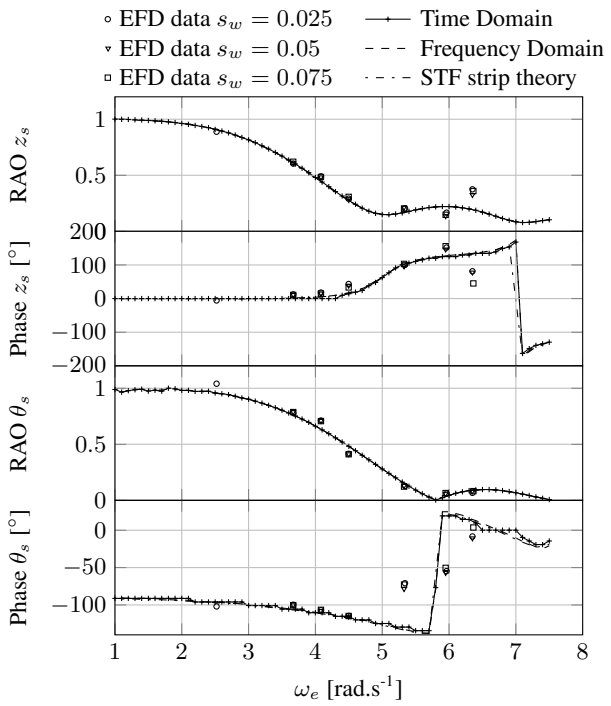

Figure 4: Heave and pitch transfer function at $U = 0.0$ m.s^{-1}as function of the frequency of encounter w_e. The results are obtained with the frequency domain and time domain approaches, experimental data for different wave steepness s_w and with the STF strip theory.

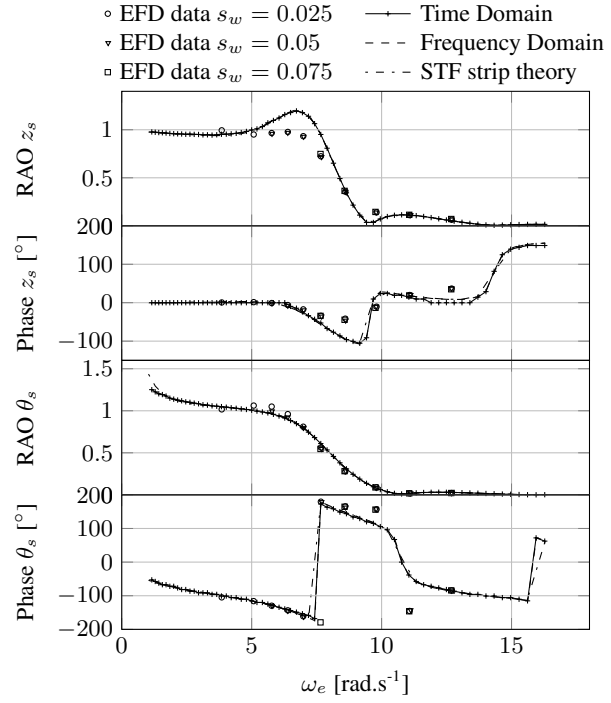

Figure 5: Heave and pitch transfer function at $U = 1.53$ m.s^{-1} as function of the frequency of encounter w_e. The results are obtained with the frequency domain and time domain approaches, experimental data for different wave steepness s_w and with the STF strip theory.

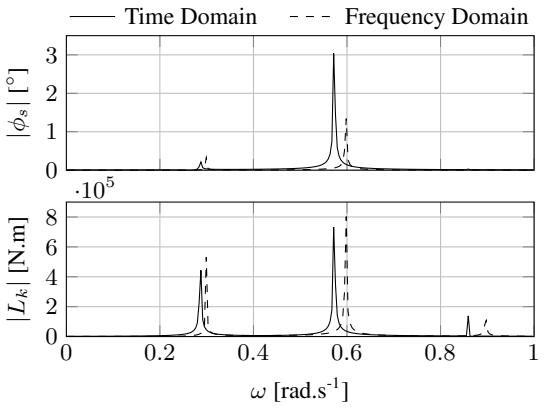

Figure 6: In calm water, the ship roll motion spectrum is plotted at the top and the kite heeling moment excitation spectrum is plotted at the bottom; the frequency domain approach is represented by the dashed line and the time domain approach is represented by the solid line.

4 SHIP TOWED BY KITE: TIME DOMAIN APPROACH VERSUS FREQUENCY DOMAIN APPROACH

In this section, the time and frequency domain approaches are compared in term of ship motions spectrum and kite excitation spectrum. The full scale DTMB 5512 is considered on a crosswind path. The ship speed is 7.5 m.s^{-1}. The wind velocity is 7.5 m.s^{-1}. The ship is towed by a kite of 500 m^{2}and 500 m tether length. The considered lift to drag angle is 9.6 for a lift coefficient of 0.7. The kite performs a dynamic flight of an elevation amplitude of $\Delta\theta_8 = 20°$ and of an azimuth amplitude of $\Delta\phi_8 = 8°$, centered on $[\theta_8, \phi_8] = [28.2°, 57.6°]$, and rotated by an angle $\chi_8 = 70.1°$. These trajectory parameters have been computed according to the optimisation of R. Leloup et al. in [1] in order to maximize the towing force along the longitudinal axis of the ship. The following simulations are performed leaving free the heave, roll and pitch motions and constraining the horizontal motions. The presented results are focused on the roll motion.

4.1 RESULTS

Figures 6 and 7 show the spectrum of the amplitude of the roll motion on the top and the spectrum of the kite moment around $\underline{x}_s$ at the bottom. Figure 6 correponds to a calm water case, while Fig. 7 corresponds to a case with a beam wave of an amplitude of 3 m and of a frequency of 0.4 rad.s^{-1}.

The kite excitation for the frequency domain approach is first computed into the time domain over 1100 s of simulation with a time step of 0.1 s. Then only the last 1024 s of simulation are considered to perform the FFT of the signal. The same procedure is performed to obtain the spectrum of the time series obtained with the time domain approach. Consequently, the spectral resolution of the spectrums in Figs. 6 and 7 is $6{\cdot}10^{-3}$rad.s^{-1}. Over 1 rad.s^{-1}, the spectrums are not represented since the amplitudes decrease drastically.

The maximum roll motion amplitude obtained with the

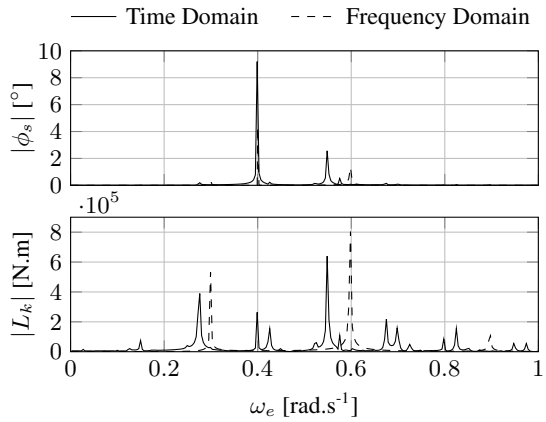

Figure 7: With a beam wave of 3 m height and of 0.4 rad.s^{-1} of frequency, the ship roll motion spectrum is plotted at the top and the kite heeling moment excitation spectrum is plotted at the bottom; the frequency domain approach is represented by the dashed line and the time domain approach is represented by the solid line.

time domain approach is 3.75° around mean heeling angle of 0.90° in calm water. Performing an inverse FFT of the roll motion spectrum obtained with the frequency domain approach, the maximum roll motion amplitude is 1.68°. For the beam wave case in Fig. 7, the maximum roll amplitude motion is 12.65° for the time domain approach whereas for the frequency domain approach the maximum roll amplitude is 6.21°.

4.2 ANALYSIS

4.2.1 Calm Water Case

The bottom of Fig. 6 shows that kite excitation spectrum is composed of mainly three peaks, leading to three peaks for the roll motion spectrum concerning the frequency domain and time domain approaches. The results show that these peaks are at lower frequencies in case of the time domain approach than in case of the frequency domain approach. These frequency gaps of the peaks between the two approaches seem to increase with the frequency. Indeed, for the first peak, a gap of $1{\cdot}10^{-2}$rad.s^{-1} is observed whereas this gap increases to $3{\cdot}10^{-2}$rad.s^{-1} for the second peak and to $4{\cdot}10^{-2}$rad.s^{-1} for the third peak.

The amplitude of the roll motion should be compared to the natural roll frequency of the ship which is 0.54 rad.s^{-1}. The closer to the roll natural frequency the peak is, the more important the amplitude of the roll motion is. Consequently, an important roll motion can be observed for the second peak for the two approaches. For the frequency domain approach, the second peak at $5.9{\cdot}10^{-1}$ rad.s^{-1} has an amplitude of 1.34°. For the time domain approach, the peak at $5.7{\cdot}10^{-1}$ rad.s^{-1} is closer to the natural frequency and the roll amplitude is 3.04°. The amplitude predicted by the time domain approach is more than twice the amplitude of the second peak of the frequency domain approach.

On the contrary, the first peak is closer to the natural roll frequency in case of the frequency domain approach than in case of the time domain approach. Thus, the roll motion amplitude is greater for the frequency domain approach than for the time domain approach.

4.2.2 Beam Wave Case

In Fig. 7, the roll amplitude due to kite excitation of the frequency domain approach remains unchanged compared to the case in calm water case. A peak at $4.0{\cdot}10^{-1}$ rad.s^{-1}appears due to the wave excitation. The roll motion amplitude due to the wave is 4.34°.

With the time domain approach, Fig. 7 shows that the presence of a wave modifies a lot the kite excitation spectrum. Several peaks of excitation appear. It can be highlighted that a peak of excitation appears at the wave frequency. The resulting roll amplitude spectrum is significantly affected. Indeed, the roll motion spectrum is dominated by the wave excitation with a peak at 0.4 rad.s^{-1} of a magnitude 9.20°.

Regarding the calm water case, the same peaks are present. However, the kite excitation amplitude for these peaks are lower. For instance, the second peak, the kite excitation amplitude in calm water is of $7.31{\cdot}10^5$N.m in calm water whereas it is $6.39{\cdot}10^5$N.m for the beam wave case. The resulting roll motion amplitude for the peak at $5.48{\cdot}10^{-1}$ rad.s^{-1} is 2.57° with the beam wave case against 3.04° in calm water.

4.3 DISCUSSION

The differences between the frequency domain approach and the time domain approach are due to the level of coupling between the kite and the ship model. For the frequency domain approach the kite excitation is computed considering the mean ship speed. There is no interaction between the ship and the kite model. On the contrary, using the time domain approach, a strong coupling between the ship and the kite is performed.

In case of calm water and with the time domain approach it can be clearly noticed that the frequency of the kite excitation decreases due to the ship motion. The resulting roll motion amplitude doubles compare to the frequency domain approach. This important difference on the roll amplitude can be explained by the proximity natural roll frequency of the ship. Indeed, with the strong coupling, the frequency of the kite excitation decreases and is closer to the natural frequency.

The lower frequency of the kite excitation with the strong coupling compared to the weak coupling into the frequency domain can be explained either by the natural roll ship frequency or by the ship roll motion. This suggests to investigate different trajectories or tether lengths in order to shift the frequency of the kite excitation at a lower frequency than the natural ship frequency.

The results with a beam wave highlight the importance to model the interaction between the kite and the ship. The kite excitation is highly modified by the presence of wave. Consequently, it appears a peak of frequency in the kite spectrum at the wave frequency. Thus, the roll amplitude doubles with the strong coupling compared to the weak frequency coupling.

In this study, in order to assure the feasibililty of the kite flight, the trajectory has been defined with respect to the rela-

tive wind frame. Nevertheless, this frame moves with the ship motions. Consequently, this could explained the important modification of the kite excitation due to the ship motion. Further studies should be performed to investigate the influence of the kite control. Moreover, the horizontal ship motions has been constrained in this study. The sway motion may have an important effect on the roll motions due to the transverse kite force and the wave the drift force.

Despite the questionable assumptions mentioned before, it appears necessary to perform a strong coupling between the ship and the kite, especially in presence of waves. The presented study shows important differences between the weak and the strong coupled model in calm water as well. Nevertheless, the difference between the two model seems to be severally increased by the proximity of the natural roll ship frequency. Consequently, further investigations should be performed to assess the quality frequency domain approach far from the natural roll ship frequency. This can be motivated by the very short computing time of the frequency domain approach. Even if the time domain approach is faster than the real time, the frequency domain approach is even faster.

5 CONCLUSION

A time domain approach and a frequency domain approach have been developed to model the dynamic of ship towed by kite in waves. The time domain approach is based on the Cummin's equation. The convolution product has been performed using state-space models. The state-model models have been identified with the STF strip theory using a method mixing time domain and frequency domain identifications. The kite has been modeled with an analytical formulation of the so-called zero mass model. A strong coupling between the kite and the ship is performed with the time domain approach whereas a weak coupling is employed with the frequency domain approach.

A validation using EFD data has been perfomed on the DTMB 5512 in monochromatic head waves. The results show that the heave and pitch motions predicted by the STF strip theory and the time domain and frequency domain approaches are consistent. Their comparisons with the EFD data are satisfactory. The approximations performed using state-space models are negligible.

On the DTMB 5512 at full scale with a kite of 500 m^2 a comparison of the time domain and the frequency domain approaches have been compared in calm water and with a beam wave to assess the importance of performing a strong coupling. The results show that a strong coupling is necessary with waves. The heeling angle predicted with the time domain approach is higher than twice the heeling angle predicted by the frequency domain approach. In calm water, the same observation can be made. Nevertheless it must be noticed that it may be due the fact that the kite excitation frequency and the natural roll frequency were closed.

6 ACKNOWLEDGMENTS

The authors are grateful to the French Environment and Energy Management Agency (ADEME) for its financial support.

7 AUTHORS BIOGRAPHY

N. Bigi is currently following a Ph.D. Degree at the Dupuy de Lôme Research Institute at the graduate and post graduate school of engineering, Ecole Nationale Supérieure de Techniques Avancées Bretagne (ENSTA Bretagne), Brest, Brittany, France. Previously, he worked for HDS Design (recently merged with GSEA Design) to develop a fluid structure interaction program and a 3D lifting line method dedicated to the appendages of racing yachts at the early design stage. He graduated at ENSTA Bretagne in 2014 in naval architecture and offshore engineering.

J. B. Leroux is Associate Professor of Naval Hydrodynamics at the graduate and post graduate school of engineering, Ecole Nationale Supérieure de Techniques Avancées Bretagne (ENSTA Bretagne), Brest, Brittany, France. He is currently in charge of fluid mechanics courses. He received his Ph.D. degree (2003) with Honours from the University of Nantes, France. His research skills mainly cover cavitation and hydrodynamics instabilities.

K. Roncin is Associate Professor of Naval Hydrodynamics at the graduate and post graduate school of engineering, Ecole Nationale Supérieure de Techniques Avancées Bretagne (ENSTA Bretagne), Brest, Brittany, France. He is currently the head of the Master of Science in Naval Hydrodynamics and gave during several years specialized lectures in naval construction and design. He received his Ph.D. degree (2000) with Honours from the University of Nantes, France. His research skills cover seakeeping, manoeuvrability and sail yacht dynamics.

A. Nême is Associate Professor of Engineering and Materials Science at the graduate and post graduate school of engineering, Ecole Nationale Supérieure de Techniques Avancées Bretagne (ENSTA Bretagne), Brest, Brittany, France. He is currently in charge of mathematics and strength of materials courses. He received his Ph.D. degree (1994) with Honours from the Ecole Normale Supérieure de Cachan, France. His research skills mainly cover linear and non-linear analysis in structural engineering.

C. Jochum is Associate Professor of Mechanical Engineering and Materials Science at the graduate and post graduate school of engineering, Ecole Nationale Supérieure de Techniques Avancées Bretagne (ENSTA Bretagne), Brest, Brittany, France. He worked several years in the Industry as head of the research department for a French supplier of track maintenance and construction equipment, involved in rigid body mechanics and structures design. He received his Ph.D. degree (1999) with Honours from the University of Metz, Lorraine, France. His research skills cover thermosetting

composites from multiphysics couplings and internal stress issues to dynamical behaviour and strengthening.

Y. Parlier has succeeded brilliantly in all the major nautical races and has strived throughout his life to promote respect for man and the environment. He has a graduate degree in composite materials and launched several innovations in sail yacht design. We remember the Vendée Globe 2000 when all alone, near an island off New Zealand, he successfully rebuilt and erected a new mast and finished his round the world voyage. Taking advantage of wind energy by using kites as auxiliary propulsion device is the aim of the "Beyond the sea" project launched by Yves Parlier.

REFERENCES

[1] R. Leloup, K. Roncin, M. Behrel, G. Bles, J.-B. Leroux, C. Jochum, and Y. Parlier. A continuous and analytical modeling for kites as auxiliary propulsion devoted to merchant ships, including fuel saving estimation. *Renewable Energy*, 86:483–496, 2016.

[2] P. Naaijen, V. Koster, and R. P. Dallinga. On the power savings by an auxiliary kite propulsion system. *International shipbuilding progress*, 53:255–279, 2006.

[3] N. Bigi, M. Behrel, K. Roncin, J. B. Leroux, A. Nême, C. Jochum, and Y. Parlier. Course Keeping of Ship Towed by Kite. In *15e Journées de l'Hydrodynamique*, pages 1–14, 2016.

[4] Renato Skejic. Ships Maneuvering Simulations in a Seaway - How close are we to reality ? pages 91–101, 2013.

[5] WE Cummins. The impulse response function and ship motions. Technical report, DTIC Document, 1962.

[6] PA Bailey, WG Price, and P Temarel. A unified mathematical model describing the manoeuvring of a ship travelling in a seaway. *Trans. RINA*, 140:131–149, 1997.

[7] Erlend Kristiansen, Asmund Hjulstad, and Olav Egeland. State-space representation of radiation forces in time-domain vessel models. 32:2195–2216, 2005.

[8] Thor I. Fossen and Øyvind N. Smogeli. Nonlinear time-domain strip theory formulation for low-speed manoeuvring and station-keeping. *Modeling, Identification and Control*, 25(4):201–221, 2004.

[9] J. F. Wellicome and S. Wilkinson. Ship propulsive kites: an initial study. *Department of Ship Science, University of Southampton*, 1984.

[10] G. M. Dadd, D. A. Hudson, and R. A. Shenoi. Determination of kite forces using three-dimensional flight trajectories for ship propulsion. *Renewable Energy*, 36(10):2667–2678, oct 2011.

[11] The University of Iowa. EFD Data.

[12] M Irvine, J Longo, and F Stern. Pitch and Heave Tests and Uncertainty Assessment for a Surface Combatant in Regular Head Waves. *Journal of Ship Research*, 52(2):146–163, 2008.

[13] T.I. Fossen. A Nonlinear Unified State-Space Model for Ship Maneuvering and Control in a Seaway. *International Journal of Bifurcation and Chaos*, 15(09):2717–2746, 2005.

[14] Francis T. Ogilvie. Recent Progress Towards the Understanding and Prediction of Ship, 1964.

[15] N. Salvesen, Eo Tuck, and O. Faltinsen. Ship motions and sea loads. *Trans. SNAME*, 78:250–287, 1970.

[16] J. N. Newman. *Marine Hydrodynamics*. MIT Press, 1977.

[17] Tristan Pérez and Thor I. Fossen. Time-vs. frequency-domain Identification of parametric radiation force models for marine structures at zero speed. *Modeling, Identification and Control*, 29(1):1–19, 2008.

[18] S. Y. Kung. A New Identification and Model Reduction Algorithm via Singular Value Decompositions. In *Twelfth Asilomar Conference on Circuits, Systems and Computers*, pages 705–714, 1978.

[19] M. Greenhow. High- and low-frequency asymptotic consequences of the Kramers-Kronig relations. *Journal of Engineering Mathematics*, 20:293–306, 1986.

[20] ITTC Symbols and Terminology List Version 2014. Technical report, 2014.